Synthesis and Characterization of Taper- and Rodlike Si Nanowires on Si_XGe_{1-X} Substrate

Y. L. Chueh,[†] L. J. Chou,*[,†] C. M. Hsu,[‡] and S. C. Kung[‡]

Department of Materials Science and Engineering, National Tsing-Hua University, Hsinchu, Taiwan, Republic of China, and Industrial Technology Research Institute, Hsinchu, Taiwan, Republic of China

Received: July 10, 2004; In Final Form: July 3, 2005

Taper- and rodlike Si nanowires (SiNWs) are synthesized successfully on Si and $Si_{0.8}Ge_{0.2}$ substrates. The growth mechanisms of taper- and rodlike SiNWs are proposed to be oxide-assisted growth (OAG) and vapor−liquid−solid (VLS) growth, respectively. For taperlike SiNWs annealed at 1200 °C for 3 h, the emission peaks are found at 772, 478, and 413 nm. On the other hand, for rodlike SiNWs annealed at 1200 °C for 4 h, emission peaks are found at 783, 516, and 413 nm. From the field-emission measurements, the taperlike Si nanowires exhibit superior field-emission behavior with a turn-on field of 6.3−7.3 V/μm. The field enhancement, β, has been estimated to be 700 and 1000 at low and high fields, respectively. The excellent field-emission characteristics are attributed to the perfect crystalline structure and the taperlike geometry of the Si nanowires.

1. Introduction

One-dimensional (1D) systems such as nanowires, nanorods, nanobelts, and carbon nanotubes (CNTs) have attracted much attention owing to their unique optical, electronic, and mechanical properties.[1,2] However, silicon nanowires (SiNWs) are important semiconducting nanowires with unique sp^3-bonded crystal structure and relatively low work function. Growth mechanisms of SiNWs, including vapor−liquid−solid growth (VLS),[3,4] solid−liquid−solid growth (SLS),[5] and oxide-assisted growth (OAG),[6−8] have been widely proposed and discussed. In the VLS model, the anisotropic crystal growth is guided by precipitated liquid droplets. The droplet surface possesses a high sticking coefficient, which provides an absorption site for the vapor reactant to reach a supersaturation state. Accordingly, nanowires are generated by means of segregation out of the droplet surface. The VLS growth process is also called the catalysis growth. OAG emphasizes that the formation of an unstable oxide phase is essential. The nucleation at low temperature is achieved by the decomposition of unstable oxide, and the temperature fluctuation provides a driving force for the growth of nanowires.

In this study, we present a method for fabrication of SiNWs. β-$FeSi_2$ nanodots embedded on the Si and the $Si_{0.8}Ge_{0.2}$ substrate were annealed to grow Si nanowires at elevated temperature in a N_2 ambient. Two different morphologies of SiNWs are found. One is the taperlike SiNWs grown on the Si substrate. The other is the rodlike Si nanowires, which are free of metal catalyst. The taperlike structure has been found on several materials, such as CNT, ZnO, CdO, and IrO_2.[9−12] However, a similar structure has not been found in the previous SiNWs reports. The optical and electrical properties of these SiNWs have been examined in detail, and the possible growth mechanisms for these taperlike and rodlike SiNWs are proposed.

* Corresponding author. E-mail: ljchou@mx.nthu.edu.tw.
[†] National Tsing-Hua University.
[‡] Industrial Technology Research Institute.

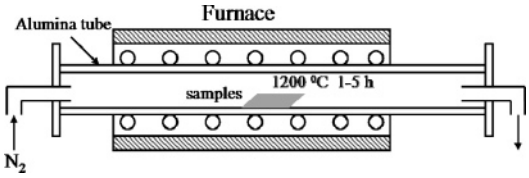

Figure 1. Schematic diagram of the apparatus for synthesis of taper- and rodlike SiNWs.

2. Experimental Methods

Two types of substrates used for this experiment are Si and SiGe substrates. The Si substrates used are single crystal (001) Si (1−30 Ω cm) substrates. Virtual $Si_{0.8}Ge_{0.2}$ substrates are prepared by expitaxially depositing a 200 nm thick Si buffer layer on a single-crystal (001) Si substrate at 500 °C using ultrahigh-vacuum vapor deposition (UHV-CVD), then a 800 nm thick $Si_{0.8}Ge_{0.2}$ film is deposited epitaxially by UHV-CVD. The two types of substrates (Si and $Si_{0.8}Ge_{0.2}$) are deposited as a 4 nm thin amorphous Si (a-Si) layer, followed by depositing a 1.5 nm thin Fe film using an ultrahigh-vacuum electron beam system at room temperature. The as-deposited samples are then annealed at 800 °C for 2 h in a vacuum at a pressure lower than 10^{-8} Torr without breaking the vacuum to form β-$FeSi_2$ nanodots on the Si and the $Si_{0.8}Ge_{0.2}$ substrate. Subsequently, these samples are annealed in a furnace at 1100−1200 °C for 1−5 h in a N_2 ambient, as shown in Figure 1. A field-emission transmission electron microscope (JEM-3000F, operating at 300 kV with point-to-point resolution of 0.17 nm), equipped with an energy dispersion spectrometer (EDS), is used for the microstructure and the chemical composition analysis. The surface morphology is examined with a field-emission scanning electron microscope (JSM-6500F, operating at 15 kV). Photoluminescence (PL) is performed at room temperature using a He-Cd laser with a wavelength of 325 nm as the excitation source, and the PL signal is amplified using a photon multiplier tube (PMT). The electron field-emission property of SiNWs is measured in a vacuum chamber at a vacuum pressure of 1×10^{-7} Torr using a spherical stainless steel probe (1 mm in diameter) as the anode. The lowest emission current has been

10.1021/jp046945a CCC: $30.25
Published on Web 10/21/2005

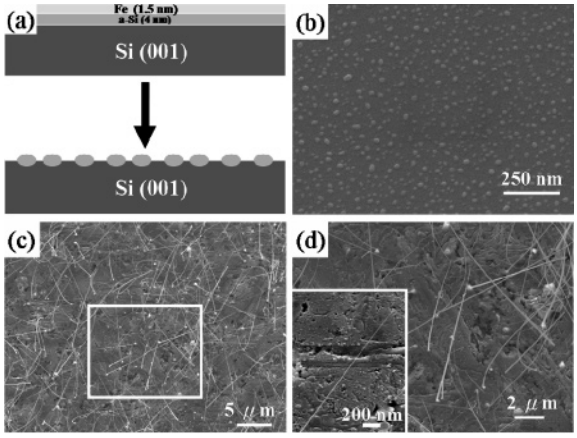

Figure 2. (a) Schematic illustration of the Fe/a-Si/Si (001) samples forming the $FeSi_2$ nanodots on the Si substrate after annealing in a vacuum at 800 °C for 5 h. (b) SEM image of an Fe (1.5 nm)/a-Si(4 nm)/Si(001) sample annealed in a vacuum at 800 °C for 5 h. (c) Plane-view SEM images of taperlike Si nanowires. (d) Plane-view SEM image of taperlike Si nanowires. Inset shows a magnified SEM image of the tip region.

recorded at nA level. The measurement distance between the anode and the emitting surface is fixed at 50 μm.

3. Results and Discussion

3.1. Taperlike Si Nanowires. Figure 2a illustrates the process in which nanodots are grown on the Si substrate after annealing in a vacuum at 800 °C for 2 h. The SEM image reveals that the substrate surface is decorated with dome-shaped nanodots of 20−30 nm in diameter (Figure 2 b). Figure 2c shows a SEM image of tapered SiNWs, which are formed by annealing nanodots at 1200 °C for 3 h in a N_2 ambient. Another observation is the appearance of voids on the surface of the Si substrate (Figure 2c,d). Figure 2d shows the enlarged SEM view of the boxed area shown in Figure 2c. The magnified SEM image of the tapered feature is also shown in the inset of Figure 2c. The tip and the bottom of the tapered wires are about 5−10 and 40−55 nm in diameter, respectively, and they are about 5−6 μm long with an aspect ratio of about 150−170.

The TEM image of the SiNW, as shown in Figure 3a, indicates that the diameter of the Si core is 25 nm with a silicon oxide coating layer of 3−4 nm. The TEM/EDS quantitative measurement shows that the oxide coating layer of the SiNW has an atomic ratio of 1:2 (Si/O). Figure 3b displays the corresponding high-resolution TEM image with [111] zone axis. The growth direction of the taperlike Si nanowire (i.e., nanowire axis) is along the $[11\bar{2}]$ crystalline direction. The crystal plane perpendicular to the crystal growth is the {111} facet plane, which has the lowest surface energy. In addition to the growth of the nanowire along the $[11\bar{2}]$, the growth direction along [110] is also observed. Figure 3c shows the EDS line profile at the tip region, indicating that the tip consists of Si and O only. TEM/EDS quantitative measurements, as shown in Figure 3d, indicate that the atomic percentages of Si and O are 44% and 56%, respectively. Figure 3e displays the line profiles across the nanowire. The absence of Fe in the nanowires is attributed to the evaporation of Fe-containing compounds during the high-temperature process.

3.2. Rodlike Si Nanowires. Nanodots are grown on the $Si_{0.8}Ge_{0.2}$ substrate using the same approach, as shown in Figure 4a. The uniformly distributed dome-shaped nanodots are partially embedded on the $Si_{0.8}Ge_{0.2}$ substrate with a diameter of about 40−50 nm. From the TEM/EDS measurements, the atomic percentages of these nanodots for Fe, Si, and Ge are 30%, 65%, and 5%, respectively. The phase has been identified as $Fe(Si_xGe_{1-x})_2$, suggesting that some Ge atoms are involved in the silicidation process. No segregation of Ge atoms from $Fe(Si_xGe_{1-x})_2$ at the interface is detected. Figure 4b−d shows nanowires that are grown on the $Si_{0.8}Ge_{0.2}$ substrate at 1200 °C for 1, 2, and 4 h. After annealing at 1200 °C for 1 h, rodlike nanowires have metal catalysts at the tip regions. The nanowires would continue to grow in length by increasing the annealing time. Nevertheless, as the annealing time approaches 2 h, a necking phenomenon begins to appear between the metal catalyst and the rodlike body, as shown in Figure 4c. The magnified SEM image (inset in Figure 4c) clearly shows the formation of a necking structure. As the annealing time increase to 4 h, the metal catalysts mostly fall off from the tip regions, as shown in Figure 4d.

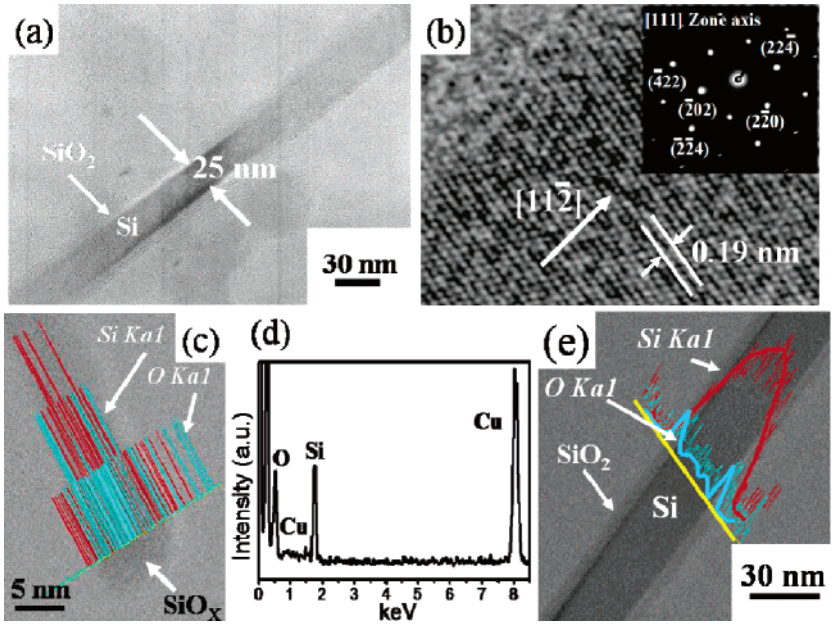

Figure 3. (a) TEM image of the taperlike Si nanowire. (b) High-resolution TEM image of a taperlike Si nanowire. The growth is along the $[11\bar{2}]$ direction. Inset shows the corresponding selective area diffraction (SAD) pattern of the [111] zone axis. (c) EDS line profile showing that the tip region consists of Si and O. (d) Corresponding EDS spectrum for the tip region of the nanowire. (e) EDS line profiles of the nanowire.

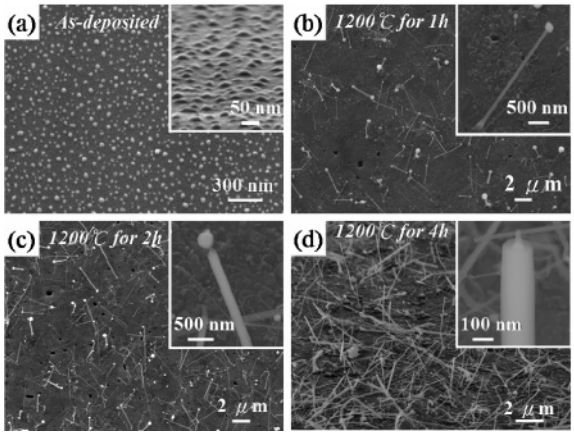

Figure 4. (a) SEM image of an Fe (1.5 nm)/a-Si (4 nm)/$Si_{0.8}Ge_{0.2}$ (001) sample annealed in a vacuum at 800 °C for 5 h. Inset shows the magnified SEM image. (b) SEM image of the rodlike SiNW grown from $Fe(Si_xGe_{1-x})_2$ nanodots with a metal catalyst at the tip region annealed at 1200 °C for 1 h. Inset shows the magnified SEM image. (c) SEM image of the necking phenomenon of the rodlike SiNW annealed at 1200 °C for 2 h. Inset shows the magnified SEM image. (d) SEM image of the rodlike SiNWs without metal catalyst on the tip area annealed at 1200 °C for 4 h. Inset shows the magnified SEM image.

Figure 5a shows a TEM image of the rodlike Si nanowires annealed at 1200 °C for 2 h. The diameter of the nanowire is about 100 nm with the metal catalyst on the tip region. The high-resolution TEM image and the corresponding electron diffraction pattern (SAD) with the [211] zone axis are shown in Figure 5b, revealing that the growth direction of the SiNW is along [111]. The EDS line profiles, as shown in Figure 5c−e, show that the metal catalyst is composed of Si, Fe, and Ge, and the wire core is made of Si only. Note that an amorphous layer of about 1−2 nm, consisting of Si and O, is also observed, as shown in Figure 5e. The atomic ratio for the amorphous thin layer is about 1:1 (Si:O), as determined by TEM/EDS measurements.

3.3. Growth Mechanisms. Previous studies suggested that the [111] growth direction of the SiNWs is a metal-catalytic VLS process.[3,4] On the other hand, for the oxide-assisted growth mechanism (OAG), the growth direction of the SiNWs is preferred along ⟨112⟩ or ⟨110⟩.[7,8] The absence of metal catalyst on the tip region is mainly because the VLS growth mechanism does not apply to the taperlike SiNWs' growth. The growth model for the taperlike SiNWs is proposed on the basis of the SEM images (Figure 2) and the TEM images (Figure 3). The growth model is illustrated in Figure 6a−c. The eutectic point of bulk $FeSi_2$ is 1207 °C. Due to the size effect,[13] $FeSi_2$ nanoparticles are prone to the molten state at 1200 °C in the initial annealing stage, but before the tapered wire growth begins (Figure 6a). The relatively high solubility of Si atoms in the binary $FeSi_2$ phase enables the diffusion of Si atoms into $FeSi_2$ droplets (1SL interface, Figure 6b) from the solid substrate, and a supersaturation state is established. A temperature gradient across the molten catalyst induces Si atoms to precipitate on top of the $FeSi_2$ droplets; consequently, a second liquid−solid interface (2LS interface, Figure 6b) is formed, which is a typical solid−liquid−solid (SLS) growth mechanism. The $FeSi_2$ droplets are gradually vaporized during the annealing process. At the same time, the residual O will react with the Si substrate to form SiO_2 and SiO. The unstable SiO phase would be easily vaporized and condense onto the surface of the growing wires (Figure 6c). The Si atoms segregate from SiO_X and attach to the Si nanowires along the [112] or [110] direction during the annealing process (Figure 6c). The OAG mechanism dominates the nanowire growth. The surface layer of the wire is oxidized, forming an oxide sheath, which will limit the growth in the lateral direction. The suggested chemical reactions of taperlike SiNWs are as follows:

$$2SiO \rightarrow 2SiO_X + (1 - X)O_2 \quad (1)$$

$$SiO_X \rightarrow (1 - X)Si + XSiO \quad (2)$$

It is suggested that the different absorption of SiO along the nanowire axis may result in the taperlike morphology. The taperlike SiNWs will continue to grow as the annealing time proceeds. No growth of SiNWs is detected for samples annealed at 1100 °C.

For taperlike SiNWs, SiOx catalysts found at the tip region indicate that a possible growth mechanism may be dominated

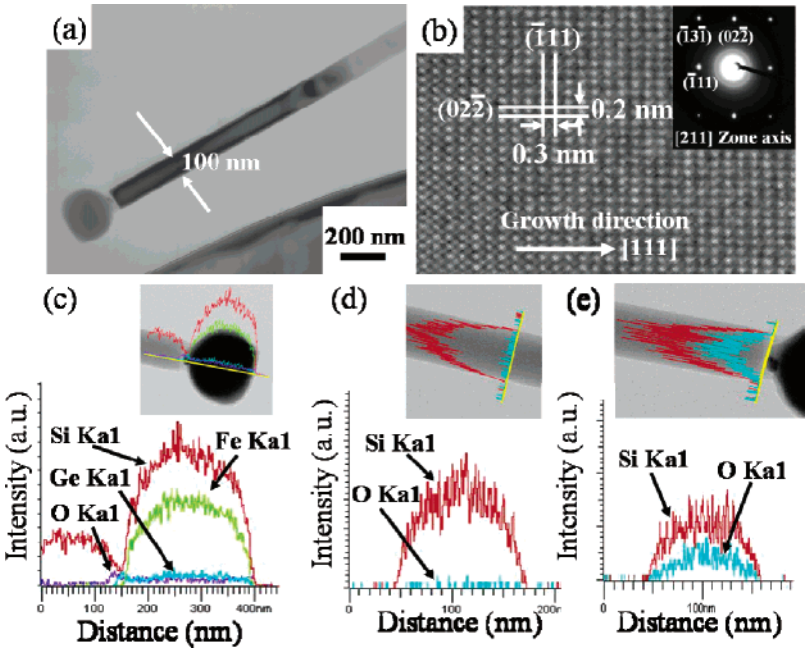

Figure 5. (a) TEM image of a rodlike SiNW annealed at 1200 °C for 2 h. (b) High-resolution TEM image and corresponding diffraction pattern (DF) images of the rodlike SiNWs annealed at 1200 °C for 2 h. (c−e) EDS line profiles for different regions of the rodlike SiNW.

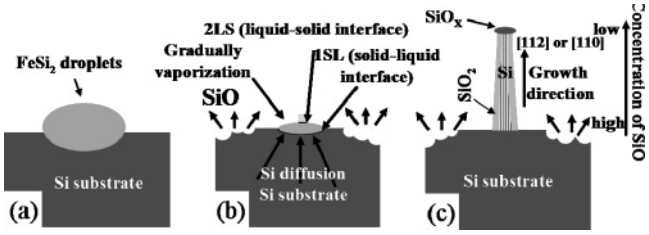

Figure 6. (a−c) Schematic illustrations for the growth of taperlike SiNWs on the Si substrate.

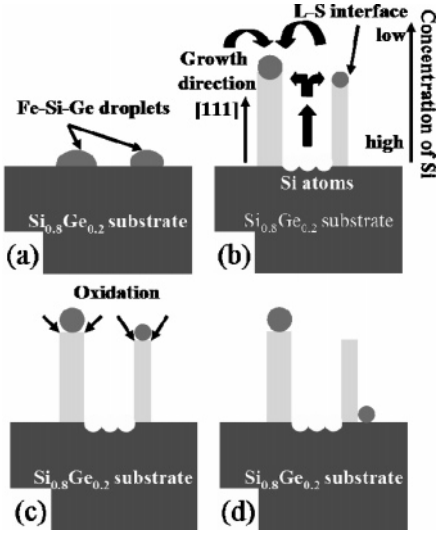

Figure 7. (a−d) Schematic illustrations for the growth of rodlike SiNWs on the $Si_{0.8}Ge_{0.2}$ substrate.

by OAG. On the other hand, the rodlike SiNWs grown on $Si_{0.8}Ge_{0.2}$ substrate with metal catalysts found at the tip region would suggest that the growth mechanism is dominated by VLS in the [111] growth direction. The proposed growth mechanisms for rodlike SiNWs are shown in Figure 7a−d. In this study, we proposed the different growth mechanisms for taperlike and rodlike SiNWs, but in a similar annealing process. The different growth mechanisms can be explained by the presence of the Ge atoms in $FeSi_2$ nanodots and on the Si substrate, resulting in a change in their melting points. The melting point of $Si_{0.8}Ge_{0.2}$ is around 1200−1250 °C; Si atoms will be vaporized out of the $Si_{0.8}Ge_{0.2}$ substrate and react with $Fe(Si_xGe_{1-x})_2$ droplets to reach a supersaturation state during the annealing process (Figure 7a). Once the temperature or the compositions fluctuate, the anisotropic growth along the [111] direction occurs (Figure 7b). Moreover, additional Si atoms, which come from the $Si_{0.8}Ge_{0.2}$ substrate, will lead to the gradient concentration of Si on the $Si_{0.8}Ge_{0.2}$ substrate. Therefore, the rodlike SiNWs have a high growth rate near the $Si_{0.8}Ge_{0.2}$ substrate, but the growth rate decreases gradually away from the $Si_{0.8}Ge_{0.2}$ substrate. Meanwhile, the small amount of residual oxygen may oxidize the interface between metal catalysts and rodlike SiNWs to form a thin SiO layer during the annealing process (Figure 7c). Because the thin SiO layer is unstable at the annealing temperature (1200 °C), it will be dissolved easily. Accordingly, the rodlike SiNWs without metal catalyst on the tip region are formed (Figure 7d).

3.4. Characterizations. Parts a and b of Figure 8 show the PL spectra of taper- and rodlike SiNWs annealed at 1200 °C for 3 and 4 h, respectively. Three major peaks are found at 772, 478, and 413 nm for the taperlike SiNWs. Peaks are spotted at 784, 516, and 413 nm for the rodlike SiNWs. The peak at 413 nm appearing in both taper- and rodlike SiNWs results from

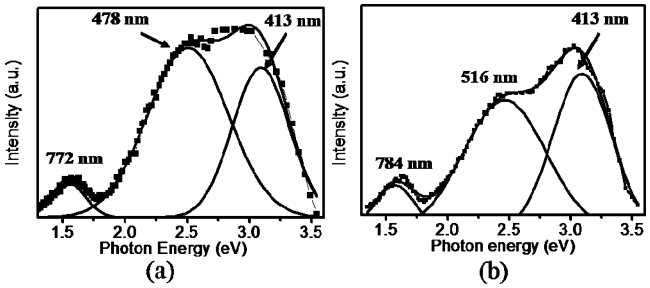

Figure 8. (a) PL spectrum of taperlike SiNW annealed at 1200 °C for 3 h. (b) PL spectrum of a rodlike SiNW without the metal catalyst at the tip region annealed at 1200 °C for 4 h.

the intrinsic diamagnetic defect center, such as the 2-fold coordinated silicon lone-pair centers (:Si:).[14] The peaks at 478 and 516 nm are attributed to the oxygen vacancy (neutral oxygen vacancy; ≡Si≡).[14−16] The peaks at 772 and 784 nm are attributed to the Si core, possibly owing to the quantum confinement effect.[17]

Parts a and b of Figure 9 show the field-emission properties measured at a separation of 50 μm between the emitting surface and the anode of the rodlike SiNWs annealed at 1200 °C for 1 and 4 h, respectively. The turn-on field intensity is defined as the electric field required for generating a current density of 0.01 mA/cm^2, which is sufficient for operating display panel devices.[18] The turn-on voltages for the rodlike Si nanowires annealed at 1 and 4 h are about 21 and 18 V/μm, respectively. Figure 8a,b reveals a linear relationship, the so-called $\ln(J/E^2) - (1/E)$ plot, indicating that the field-emission behavior follows the Fowler−Nordheim (F−N) relationship,[19] i.e., electrons tunneling through a potential barrier. The concise F−N equation is expressed as follows.[20]

$$J = (A\beta^2E^2/\Phi)\exp(-B\Phi^{3/2}/\beta E) \qquad (3)$$

where J = the current density, E = the applied filed strength, and Φ = work function. A and B are constant, corresponding to 1.56×10^{-10} [A V^{-2}(eV)] and 6.83×10^3 [V eV$^{-3/2}$(μm^{-1})], respectively. The field enhancement factor, β, reflects the degree of the field-emission enhancement of the tip shape on a planar surface. β is dependent on the geometry of the nanowire, the crystal structure, and the density at the emitting points. It can be determined by the slope of the $\ln(J/E^2) - (1/E)$ plot with a work function value of 3.6 eV.[21] Consequently, the β values are 200 and 300 for the rodlike SiNWs at 1200 °C for 1 and 4 h, respectively. The reason for the reduction of turn-on field and the increase of the β value from 200 to 300 is due to the absence of the metal catalysts at the tip region, which reduces the curvature radius of the emitting tips after annealing for 4 h. Consequently, the electric field can be increased near the tip region, resulting in not only prompting the probability of electron tunneling through the potential barrier but also reducing the turn-on field. On the other hand, the taperlike nanowires exhibit a superior field-emission performance with a turn-on voltage around 6.3−7.3 V/μm and the field enhancement factor, β, of 700 at the low-field region and 1000 at the high-field region. Comparing the previous studies,[21] the significant decrease in the turn-on voltage is attributed to the nature of the taperlike geometry. The increase of β at high field is due to the fact that emissions at high field lead to Joule's heating, which vaporizes the oxide coating and exposes the crystal nature of Si. The oxide coating layer will increase the potential barrier for electron tunneling, where it acts as a screening layer. The explanation is consistent with the presence of a low β at lower field.

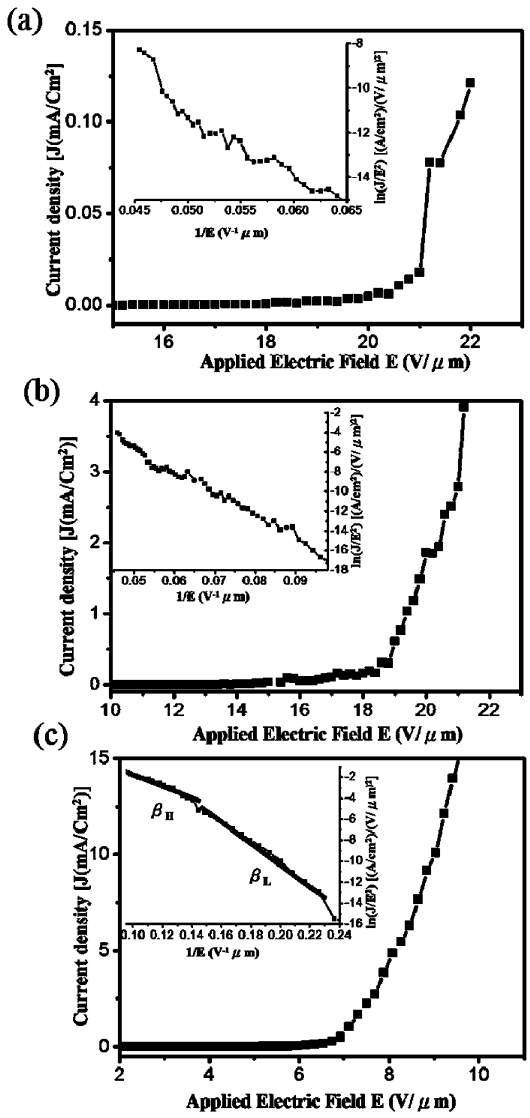

Figure 9. (a and b) Field-emission current density as a function of applied field intensity for rodlike SiNW annealed at 1200 °C for 1 and 4 h in a N_2 ambient. (c) Field-emission current density as a function of applied field intensity for taperlike SiNW annealed at 1200 °C for 3 h in a N_2 ambient.

4. Conclusions

Taper- and rodlike SiNWs have been synthesized successfully on Si and $Si_{0.8}Ge_{0.2}$ substrates after annealing in a N_2 ambient. The growth mechanisms for these two different morphologies of SiNWs have been proposed. The growth direction of the taperlike Si nanowires (i.e., nanowire axis) is along the $[11\bar{2}]$ or [110] via the OAG growth mechanism, while the growth direction along [111] for the rodlike Si nanowires is via the VLS growth mechanism. Furthermore, metal catalysts disappear during annealing due to the formation of an unstable oxide layer, which is vaporized easily during the annealing process. The optical property and the field-emission characterization of the two types of SiNWs have been carried out. For taperlike SiNW annealed at 1200 °C for 3 h, the emission peaks are at 772, 478, and 413 nm. For rodlike SiNW annealed at 1200 °C for 4 h, emission peaks are found at 783, 516, and 413 nm. For the field-emission measurements, taperlike Si nanowires exhibit a superior field emission with a turn-on field of 6.3−7.3 V/μm. The β values are 700 and 1000 at low and high fields, respectively. The excellent field-emission characteristics are attributed to the perfect crystalline structure and the taperlike geometry of the Si nanowires.

Acknowledgment. This research was supported by the National Science Council through Grant No. NSC 93-2215-E-007-012 and the Ministry of Education through Grant No. 92-I-0036-J4

References and Notes

(1) Alivisatos, A. P. *Science* **1996**, *271*, 933.
(2) Wang Q. H.; Yan, M.; Chang R. P. H. *Appl. Phys. Lett.* **2001**, *78*, 1294.
(3) Morales, A. M.; Lieber, C. M. *Science* **1998**, *279*, 208.
(4) Wu, Y. Y.; Yang, P. D. *J. Am. Soc.* **2001**, *123*, 3165.
(5) Trentler, T. J. *Science* **1995**, *270*, 1791.
(6) Wang N.; Zhang, Y. F.; Tang Y. H.; Lee, C. S.; Lee, S. T. *Appl. Phys. Lett.* **1998**, *73*, 3902.
(7) Zhang, R. Q.; Lifshitz, Y.; Lee, S. T. *Adv. Mater.* **2003**, *15*, 637.
(8) Peng, H. Y.; Pan, Z. W.; Xu, L.; Fan, X. H.; Wang, N.; Lee C. S.; Lee, S. T. *Adv. Mater.* **2001**, *5*, 317.
(9) Grobert, N.; Terrones, M.; Osborne, A. J.; Terrones, H.; Hsu, W.-K,; Trasobares, S.; Zhu, Y. Q.; Hare, J. P.; Kroto, H. W.; Walton, D. R. M. *Appl. Phys. A* **1998**, *67*, 595.
(10) Zhu, Y. W.; Zhang, H. Z.; Sun, X. C.; Feng, S. Q.; Xu, J.; Zhao, Q.; Xiang, B.; Wang, R. M.; Yu, D. P. *Appl. Phys. Lett.* **2003**, *83*, 144.
(11) Liu, X.; Li, C.; Han, S.; Han, J.; Zhou, C. *Appl. Phys. Lett.* **2003**, *82*, 1950.
(12) Liang, Y. M.; Hsieh, C. S.; Tsai, D. S.; Tiong, K. K. *Appl. Phys. Lett.* **2004**, *84*, 1552.
(13) Goldstein, A. N.; Echer, C. M.; Alivisatos, A. P. *Science* **1992**, *256*, 1425.
(14) Yu, D. P.; Hang, Q. L.; Ding, Y.; Zhang, H. Z.; Bai, Z. G.; Wang, J. J.; Zou, Y. H.; Qian, W.; Xiong, G. C.; Feng, S. Q. *Appl. Phys. Lett.* **1998**, *73*, 3076.
(15) Liao, L. S.; Bao, X. M.; Zheng, X. Q.; Li, N. S.; Min, N. B. *Appl. Phys. Lett.* **1996**, *68*, 850.
(16) Shimizu-lwayama, T.; Nakao, S.; Saitoh, K. *Appl. Phys. Lett.* **1994**, *65*, 3.
(17) Feng, S. Q.; Yu, D. P.; Zhang, H. Z.; Bai, Z. G.; Ding, Y. J. *Cryst. Growth* **2000**, *209*, 513.
(18) Wang, Q. H.; Setlur, A. A.; Lauerhaas, J. M.; Dai, J. Y.; Seelig, E. W.; Chang, R. P. H. *Appl. Phys. Lett.* **1998**, *72*, 2912.
(19) Fowler, R. H.; Nordheim, L. W. *Proc. R. Soc. London, Ser. A* **1928**, *119*, 173.
(20) Xu, C. X.; Sun, X. W. *Appl. Phys. Lett.* **2003**, *83*, 3806.
(21) Au, Frederick C. K.; Wong, K. W.; Tang, Y. H.; Zhang, Y. F.; Bello I.; Lee, S. T. *Appl. Phys. Lett.* **1999**, *75*, 1700.